

Article

# An Improved Dynamic Model and Matrix Displacement Model for Distributed-Compliance Bridge-Type Amplification Mechanism

Peixing Li <sup>1</sup>, Helei Zhu <sup>2</sup> and Leijie Lai <sup>1,\*</sup>

<sup>1</sup> School of Mechanical and Automotive Engineering, Shanghai University of Engineering Science, Shanghai 201620, China

<sup>2</sup> College of Information Science and Engineering, Jiaying University, Jiaying 314001, China

\* Correspondence: laij@suess.edu.cn; Tel.: +86-21-67874553

**Abstract:** This paper establishes a matrix displacement model and an improved dynamic model for the static and dynamic performances analysis for a kind of bridge-type displacement amplification mechanism with distributed-compliance, which has better performances than traditional lumped-compliance bridge-type mechanisms. In the matrix displacement model, the stiffness matrix for two rigid bodies connected by flexures is first obtained by regarding the displacements and the forces on two mass centers of the rigid bodies as the node displacements and node forces. By extending and superimposing each elemental stiffness matrix, the global stiffness matrix for the flexure mechanism can be obtained to calculate the displacement amplification ratio and input stiffness of the bridge-type mechanism. In the improved dynamic model, in order to establish the Lagrangian dynamic model more accurately, the deflectional, axial, and rotational velocities of any point on the beam flexure are calculated by solving the derivatives of the deformation curves of beam flexures versus time to obtain the expression of the kinetic energy in the vibrating beams. On this basis, the three-degree-of-freedom vibration differential equation for the bridge-type mechanism is established by using the Lagrange method, and the natural frequency in the working direction is obtained accurately. The presented models are compared with the finite element analysis, and experiments for two case studies of the bridge-type distributed-compliance mechanism are presented. The comparisons results demonstrate the high prediction accuracy of the improved dynamic model.

**Keywords:** bridge-type amplification mechanism; stiffness matrix; Lagrangian dynamic model; distributed-compliance



**Citation:** Li, P.; Zhu, H.; Lai, L. An Improved Dynamic Model and Matrix Displacement Model for Distributed-Compliance Bridge-Type Amplification Mechanism. *Actuators* **2022**, *11*, 368. <https://doi.org/10.3390/act11120368>

Academic Editor: Najib Kacem

Received: 19 October 2022

Accepted: 6 December 2022

Published: 7 December 2022

**Publisher's Note:** MDPI stays neutral with regard to jurisdictional claims in published maps and institutional affiliations.



**Copyright:** © 2022 by the authors. Licensee MDPI, Basel, Switzerland. This article is an open access article distributed under the terms and conditions of the Creative Commons Attribution (CC BY) license (<https://creativecommons.org/licenses/by/4.0/>).

## 1. Introduction

Piezoelectric actuators (PZTs) are widely used in the field of micropositioning/nanopositioning, which has the advantages of ultra-high resolution, high response speed, high stiffness, and high thrust [1–3]. However, the relative stroke displacement generated by PZTs is only about 10  $\mu\text{m}/\text{cm}$ , which severely limits their application range [4,5]. In view of this problem, displacement amplification mechanisms are often used to amplify the travel range of PZTs [6]. Due to the advantages of no friction, no backlash, no wear, and a compact structure, the flexure mechanism is usually used for the displacement amplification mechanism. In various amplification mechanisms, the lever-type flexure mechanisms are commonly used for the displacement amplification, but they usually have larger dimensions, low amplification ratios, and low resonant frequencies [7]. Different from the traditional lever-type mechanisms, the bridge-type mechanisms have the advantages of high amplification ratios, high resonance frequencies, and a small size, which have been used widely in modern industry [8–10].

The structure configurations and modeling methods of bridge-type flexure mechanisms have been widely studied. Lobontiu et al. used the Castigliano second theorem

to obtain an analytical model for the displacement amplification ratio and input/output stiffness calculations for the bridge-type mechanism [11]. Ma et al. derived the theoretic displacement amplification ratio of the bridge-type mechanism by using the elastic beam theory and work–energy theorem [12]. Xu et al. formulated an analytical model for the amplification ratio, input stiffness, and natural frequency calculations of a compound bridge-type amplifier based on the Euler–Bernoulli beam bending theory [13]. Liang et al. used two compound bridge-type mechanisms to design a novel monolithic two-degree-of-freedom (DOF) rotation decoupled platform [14]. Chen et al. designed and analyzed a three-dimensional bridge-type mechanism based on the stiffness distribution and the screw theory [15]. Some other bridge-type mechanisms and analytical modeling methods have also been reported [9,16–18].

Most of the bridge-type amplification mechanisms proposed in the previous studies used the notch flexure hinges for lumped-compliance. However, the large mass of rigid bodies in the traditional bridge-type mechanism with lumped-compliance has a serious impact on its dynamic performance. Instead of the notch flexure hinges used in the lumped-compliance mechanism, the distributed-compliance mechanism uses beam flexures to significantly reduce the mass of the mechanism, which can increase the natural frequency of the mechanism effectively [19,20]. In addition, different from the flexure hinge, the stress generated by the deformation of the mechanism is evenly distributed on the flexure beams; therefore, the distributed-compliance mechanism has better reliability and dynamic characteristics than the traditional lumped-compliance mechanism, especially in high-speed applications. Some amplified PZTs with the distributed-compliance mechanism have been commercialized by a number of companies including Cedrat Technologies, Core Tomorrow, etc. Even so, the static and dynamic characteristics of the bridge-type mechanism with distributed-compliance have still not been analytically modeled. Finite element analysis (FEA) is the conventional method adopted to design the mechanism's structure, and the analytical model, especially the dynamic model, has not been established in the literature. Currently, the topology-optimization-based methods for the designing of distributed compliant mechanisms are also very popular and have attracted more and more attention, because they can solve the optimal distribution of structural materials [21,22]. Therefore, in the design process, a simple and accurate analytical model is required, which can predict the performances of the flexure mechanism and determine its structural parameters according to the design specifications.

In addition, for the dynamic analysis of the flexure mechanism, the existing modeling methods are basically based on the Lagrange method, that is the kinetic energy and potential energy of the system need to be calculated, respectively. Ling et al. also proposed an extended dynamic stiffness modeling method to analyze the kinetostatic and dynamic characteristics of lumped-compliance flexure mechanisms based on d'Alembert's principle [23]. For the modeling of the lumped-compliance mechanism, the mass or the kinetic energy of the flexure hinges having a light weight and volume is usually reasonably ignored to simplify the dynamic model. Different from the lumped-compliance mechanism, in the distributed-compliance mechanism, when the beam flexure has a large thickness, its mass and kinetic energy cannot be reasonably ignored; otherwise, the modeling accuracy will be seriously reduced, which is also the difficulty in the dynamic modeling of distributed-compliance mechanisms.

For the above problems, the static and dynamic characteristics of the bridge-type displacement amplification mechanism with distributed-compliance are deeply analyzed in this paper. By using the stiffness matrix displacement method, an analytical model for the calculations of the displacement amplification ratio and input stiffness of the distributed-compliance bridge-type mechanism is established. More importantly, in order to accurately obtain the dynamic performance of the mechanism, the velocity of any point on the vibrating beam flexure is calculated to obtain the expression of the kinetic energy by solving the derivatives of the deformation curves of the beams versus time, and the natural frequency in the working direction can be obtained using the Lagrange method, which is

validated by FEA and experimental testing results. The comparisons among the analytical model, FEA results, and testing results demonstrate the high accuracy of the proposed analytical model.

The main contribution of this paper is to establish an analytical model for calculating the statics and dynamic characteristics for a class of distributed-compliance bridge-type amplification mechanisms. The static model is firstly established by using the matrix displacement method, while an improved dynamic model is formulated by considering the kinetic energy of the flexure beams in the mechanism. The modeling method and corresponding theoretical formulas of the displacement amplification ratio, input stiffness, and natural frequency proposed in this paper can accurately reveal the static and dynamic characteristics of the distributed-compliance bridge-type amplification mechanism, which provides a useful and accurate reference for the optimal designing and manufacturing of such kinds of bridge-type mechanisms.

## 2. Compliance Modeling

Figure 1 presents several typical distributed-compliance flexure mechanisms, including the traditional bridge-type amplifier, compound bridge-type amplifier, compound double-parallelogram mechanism, and cartwheel flexure mechanism. Take the bridge-type mechanism as an example; the mechanism has 4 or 8 beam flexures connected by a bridge-type structure. In this section, a matrix displacement method based on Timoshenko beam theory is derived to obtain the static and dynamic performances of the bridge-type flexure mechanisms with distributed-compliance.

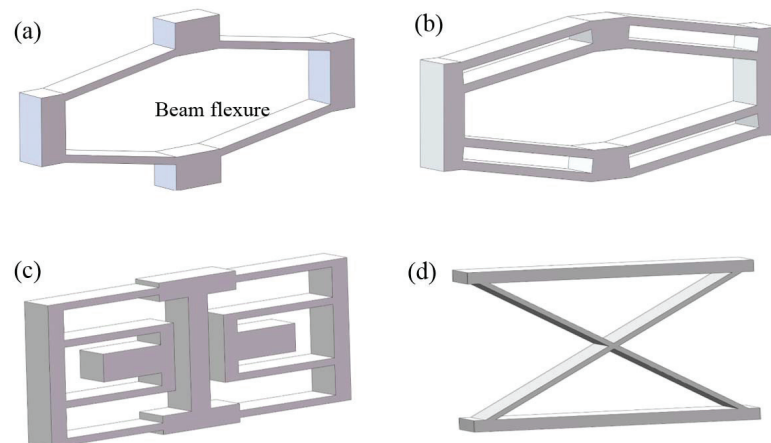


**Figure 1.** Typical distributed-compliance flexure mechanisms. (a) Traditional bridge-type amplifier. (b) Compound bridge-type amplifier. (c) Compound double-parallelogram mechanism. (d) Cartwheel flexure mechanism.

### 2.1. Beam Flexure's Stiffness Matrix

The above bridge-type distributed-compliance mechanisms are composed of multiple long beam flexures; hence, the compliance or stiffness characteristic of a beam flexure needs to be firstly calculated. Since the Timoshenko model considers the influence of the shear force on the deformation, compared with the Euler–Bernoulli model, a load–deformation relationship with higher accuracy can be calculated by the Timoshenko model. Therefore, the Timoshenko model is adopted to calculate single-beam flexure deformation for the bridge-type distributed-compliance mechanism. According to the Timoshenko beam theory, as shown in Figure 2a, the load–deformation relationship for the beam flexure is [24,25]

$$\begin{aligned} F_{xj} &= -\frac{EA}{l}u_i \\ F_{yj} &= -\frac{12EIGA}{GA l^3 + 18EI l}w_i - \frac{6EIGA}{GA l^2 + 18EI}\theta_i \\ M_{zj} &= \frac{6EIGA}{GA l^2 + 18EI}w_i + \frac{2EI(2GA l^2 - 9EI)}{GA l^3 + 18EI l}\theta_i \end{aligned} \quad (1)$$

where  $E$  and  $G$  are the elastic modulus and the shear modulus of the mechanism material.  $A = bt$  and  $I = bt^3/12$  are the cross-sectional area and the cross-section's second inertia moment, respectively.

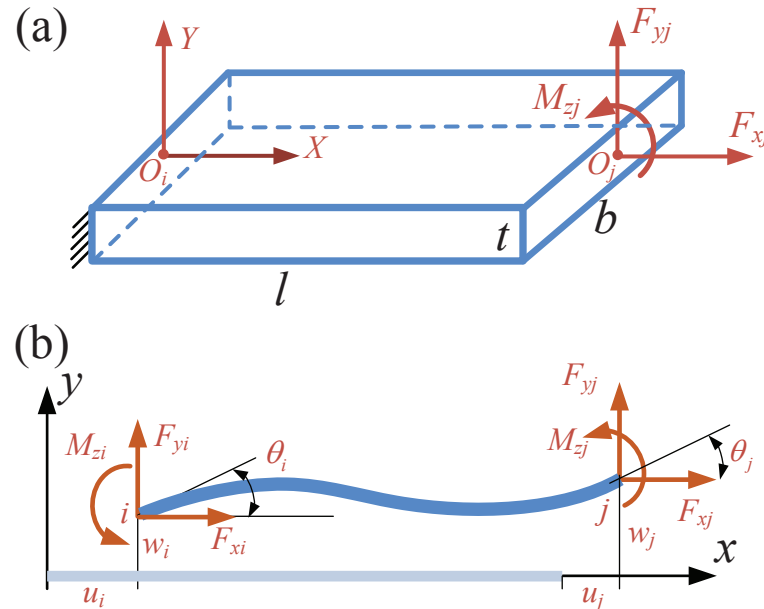


**Figure 2.** Model and deformation of a beam flexure. (a) The model of a fixed–free beam structure. (b) The model of a free–free beam structure.

By superimposing two cases of a free–fixed and fixed–free beam structure, as shown in Figure 2b, the stiffness matrix equations of a free–free beam flexure loaded at both ends is represented as

$$\mathbf{F} = \mathbf{k}\delta \tag{2}$$

where  $\mathbf{F}$  and  $\delta$  are the force and displacement vectors, respectively, expressed as

$$\mathbf{F} = [ F_{xi} \ F_{yi} \ M_{zi} \ F_{xj} \ F_{yj} \ M_{zj} ]^T$$

$$\delta = [ u_i \ w_i \ \theta_i \ u_j \ w_j \ \theta_j ]^T \tag{3}$$

The stiffness matrix for the free–free beam flexure shown in Figure 2b can be deduced as

$$\mathbf{k} = \begin{bmatrix} \frac{EA}{l} & 0 & 0 & -\frac{EA}{l} & 0 & 0 \\ 0 & \frac{12EIGA}{GAI^3+18EI} & \frac{6EIGA}{GAI^2+18EI} & 0 & -\frac{12EIGA}{GAI^3+18EI} & \frac{6EIGA}{GAI^2+18EI} \\ 0 & \frac{6EIGA}{GAI^2+18EI} & \frac{2EI(2GAI^2+9EI)}{GAI^3+18EI} & 0 & -\frac{6EIGA}{GAI^2+18EI} & \frac{2EI(2GAI^2-9EI)}{GAI^3+18EI} \\ -\frac{EA}{l} & 0 & 0 & \frac{EA}{l} & 0 & 0 \\ 0 & -\frac{12EIGA}{GAI^3+18EI} & -\frac{6EIGA}{GAI^2+18EI} & 0 & \frac{12EIGA}{GAI^3+18EI} & -\frac{6EIGA}{GAI^2+18EI} \\ 0 & \frac{6EIGA}{GAI^2+18EI} & \frac{2EI(2GAI^2-9EI)}{GAI^3+18EI} & 0 & -\frac{6EIGA}{GAI^2+18EI} & \frac{2EI(2GAI^2+9EI)}{GAI^3+18EI} \end{bmatrix} \tag{4}$$

The detailed derivation of Equations (1)–(4) can be found in [26].

### 2.2. Stiffness Matrix of Two Bodies Connected by Flexures

According to the stiffness matrix of a beam flexure with a free–free structure represented in Equations (2) and (4), the stiffness matrix of two connecting rigid bodies can be deduced. As shown in Figure 3, the  $i$ th and the  $j$ th rigid bodies are connected in parallel by  $n_{ij}$  beam flexures.

Suppose the points of  $O_i$  and  $O_j$  are, respectively, the centroids of the  $i$ th and  $j$ th rigid bodies, the relationship between the force vector  $[\mathbf{F}_{i_o} \ \mathbf{F}_{j_o}]^T$  applied to the two mass centers and the displacement vectors  $[\Delta\mathbf{q}_{i_o} \ \Delta\mathbf{q}_{j_o}]^T$  of the two points can be derived as

$$\begin{aligned} \begin{bmatrix} \mathbf{F}_{i_o} \\ \mathbf{F}_{j_o} \end{bmatrix} &= \mathbf{K}_{ij} \begin{bmatrix} \Delta\mathbf{q}_{i_o} \\ \Delta\mathbf{q}_{j_o} \end{bmatrix} = \begin{bmatrix} \mathbf{K}_{ij}^{11} & \mathbf{K}_{ij}^{12} \\ \mathbf{K}_{ij}^{21} & \mathbf{K}_{ij}^{22} \end{bmatrix} \begin{bmatrix} \Delta\mathbf{q}_{i_o} \\ \Delta\mathbf{q}_{j_o} \end{bmatrix} \\ &= \sum_{k=1}^{n_{ij}} \begin{bmatrix} \mathbf{J}_{ik} & \mathbf{0} \\ \mathbf{0} & \mathbf{J}_{jk} \end{bmatrix} \mathbf{k} \begin{bmatrix} \mathbf{J}_{ik} & \mathbf{0} \\ \mathbf{0} & \mathbf{J}_{jk} \end{bmatrix}^T \begin{bmatrix} \Delta\mathbf{q}_{i_o} \\ \Delta\mathbf{q}_{j_o} \end{bmatrix} \end{aligned} \tag{5}$$

where

$$\mathbf{J}_{ik} = \begin{bmatrix} 1 & 0 & 0 \\ 0 & 1 & 0 \\ -r_{y_{ik}} & r_{x_{ik}} & 1 \end{bmatrix} \begin{bmatrix} \cos \theta_{ik} & -\sin \theta_{ik} & 0 \\ \sin \theta_{ik} & \cos \theta_{ik} & 0 \\ 0 & 0 & 1 \end{bmatrix} \tag{6}$$

$$\mathbf{J}_{jk} = \begin{bmatrix} 1 & 0 & 0 \\ 0 & 1 & 0 \\ -r_{y_{jk}} & r_{x_{jk}} & 1 \end{bmatrix} \begin{bmatrix} \cos \theta_{jk} & -\sin \theta_{jk} & 0 \\ \sin \theta_{jk} & \cos \theta_{jk} & 0 \\ 0 & 0 & 1 \end{bmatrix} \tag{7}$$

In the above two equations,  $[\ r_{x_{ik}} \ r_{y_{ik}} \ ]^T$  ( $[\ r_{x_{jk}} \ r_{y_{jk}} \ ]^T$ ) are the vector  $\overrightarrow{O_i O_{ik}}$  ( $\overrightarrow{O_j O_{jk}}$ ) expressed in  $O_i - XY$  ( $O_j - XY$ ).  $\theta_{ik}$  ( $\theta_{jk}$ ) are the rotating angles of  $O_{ik} - XY$  ( $O_{jk} - XY$ ) with respect to  $O_i - XY$  ( $O_j - XY$ ), as shown in Figure 3.

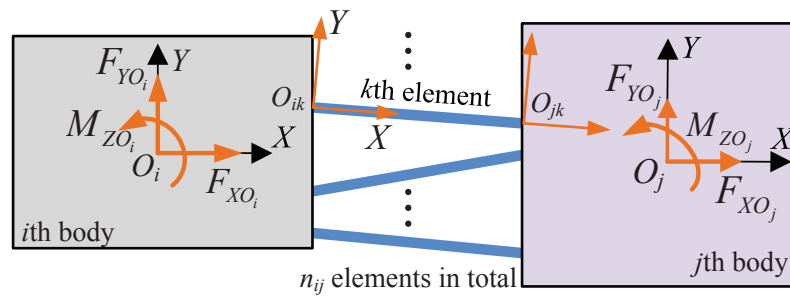


Figure 3. Two rigid bodies connected by beam flexures.

### 2.3. Global Stiffness Matrix for Flexure Mechanism

If there are  $n$  movable rigid bodies in the whole flexure mechanism,  $3n$  DOFs of the movable rigid bodies can be chosen as the generalized coordinates of the compliant mechanism if only its in-plane motion is considered. The global diagonal stiffness matrix  $\mathbf{K}$  with  $3n \times 3n$  for the flexure mechanism is established as follows.

If the  $i$ th and the  $j$ th rigid bodies are both movable, the stiffness matrix  $\mathbf{K}_{ij}$  in Equation (5) can be extended into an  $3n \times 3n$  contribution matrix  $\mathbf{K}_C$ , which can be represented as

$$\mathbf{K}_C = \begin{matrix} & \begin{matrix} 3i-2 & 3j-2 \\ \sim 3i & \sim 3j \end{matrix} \\ \begin{matrix} 3i-2 \sim 3i \\ 3j-2 \sim 3j \end{matrix} & \begin{bmatrix} \ddots & \mathbf{0} & \dots & \mathbf{0} & \ddots \\ \mathbf{0} & \mathbf{K}_{ij}^{11} & \dots & \mathbf{K}_{ij}^{12} & \mathbf{0} \\ \vdots & \vdots & \ddots & \vdots & \vdots \\ \mathbf{0} & \mathbf{K}_{ij}^{21} & \dots & \mathbf{K}_{ij}^{22} & \mathbf{0} \\ \ddots & \mathbf{0} & \dots & \mathbf{0} & \ddots \end{bmatrix} \end{matrix} \tag{8}$$

where the labels outside the matrix represent the positions of the sub-matrices in the contribution matrix. For another case of the fixed  $i$ th rigid body and movable  $j$ th rigid body, only  $\mathbf{K}_{ij}^{22}$  in the four submatrices should be extended to the  $3n \times 3n$  contribution matrix,

and vice versa. Through the above two matrix extension methods, the global stiffness matrix can be established by the superimposition of all the contribution matrices, and the load–deformation equation for the global stiffness matrix can be represented as

$$\mathbf{F} = \mathbf{K}\mathbf{q} \tag{9}$$

where  $\mathbf{q} = [\mathbf{q}_1 \ \mathbf{q}_2 \ \cdots \ \mathbf{q}_n]^T$  and  $\mathbf{F} = [\mathbf{F}_1 \ \mathbf{F}_2 \ \cdots \ \mathbf{F}_n]^T$  represent the  $3n \times 1$  displacement and force vectors of the rigid bodies in the flexure mechanism.

According to the derived stiffness matrix, the dynamic vibration equation of the flexure mechanism based on the selected generalized coordinates can be written as

$$\mathbf{M}\ddot{\mathbf{q}} + \mathbf{K}\mathbf{q} = \mathbf{F}. \tag{10}$$

where the mass matrix  $\mathbf{M}$  is

$$\mathbf{M} = \text{diag}(\mathbf{M}_1, \mathbf{M}_2, \dots, \mathbf{M}_n). \tag{11}$$

The subvector of the mass matrix is  $\mathbf{M}_i = \text{diag}(m_{xi}, m_{yi}, J_{zi})$ , where  $m_{xi}$  and  $m_{yi}$  denote the mass of the rigid body and  $J_{zi}$  is the moment of inertia about the center of mass.

The natural frequencies of the mechanism without considering the mass and vibration kinetic energy of the beam flexures can be calculated by the following two equations:

$$\det(\lambda\mathbf{I} - \mathbf{M}^{-1}\mathbf{K}) = 0 \tag{12}$$

$$f_i = \frac{1}{2\pi} \sqrt{\lambda_i}, i = 1, 2, \dots, 3n. \tag{13}$$

### 3. Improved Dynamic Model

The dynamic characteristic is an important specification in the design of compliant mechanisms. The high natural frequency of the compliant mechanism can effectively suppress external interference. Different from the lumped-compliance bridge-type mechanism, the beam flexures are used to replace the flexure hinges in the distributed-compliance mechanism. Therefore, if the mass of the beam flexures reaches a certain degree, their mass and vibration kinetic energy cannot be ignored in the process of dynamic modeling.

In order to establish the differential equation of vibration by using the Lagrange equation, the kinetic energy and potential energy of the system should be calculated first. According to the selected generalized coordinates, the kinetic energy of the rigid body can be easily obtained; therefore, this section mainly discusses the kinetic energy calculation of beam flexures. For the convenience of calculation, the beam flexure with a constant cross-section is taken as the analysis object, and its deformation is shown in Figure 4. It is assumed that the deflection curve  $w(x)$  of the beam flexures is the cubic equation of the abscissa in its local coordinate system:

$$w(x) = a_3x^3 + a_2x^2 + a_1x + a_0 \tag{14}$$

where  $a_0, a_1, a_2$  and  $a_3$  are undetermined coefficients of the deflection curve. According to the deflections and the angles at both ends of the beam flexure,  $w(0), \theta(0) = w'(0)$  and  $w(l), \theta(l) = w'(l)$ , which are expressed by the generalized coordinates of the mechanism, the coefficients of the deflection curve can be obtained as

$$\begin{cases} a_0 = w(0) \\ a_1 = \theta(0) \\ a_2 = \frac{3w(l) - 3w(0) - l\theta(l) - 2l\theta(0)}{l^2} \\ a_3 = \frac{-2w(l) + 2w(0) + l\theta(l) + l\theta(0)}{l^3} \end{cases} \tag{15}$$



where  $T_{Ri}$  is the kinetic energy of the  $i$ th rigid body,  $T_{Bj}$  represents the kinetic energy of the  $j$ th beam flexure, and  $N_R$  and  $N_B$  are, respectively, the number of rigid bodies and beam flexures in the mechanism. Both of the two kinds of kinetic energy are represented by the selected generalized coordinates in the mechanism.

According to the deformation  $\Delta l$  caused by axial tension or compression and section moment  $M(x)$  of the beam flexures, the potential energy of one beam flexure and the whole compliant mechanism can be obtained as

$$V_B = \frac{Ebt\Delta l^2}{l} + \int_0^l \frac{M^2(x)}{EI} dx, \quad V = \sum_{j=1}^{N_B} V_{Bj} \tag{23}$$

The expressions of kinetic energy and potential energy are substituted into the Lagrange equation:

$$\frac{d}{dt} \left[ \frac{\partial(T - V)}{\partial \dot{\mathbf{u}}} \right] - \frac{\partial(T - V)}{\partial \mathbf{u}} = \mathbf{f} \tag{24}$$

where  $\mathbf{u}$  and  $\mathbf{f}$  are the vectors of generalized coordinates and generalized forces, respectively. By simplifying Equation (24), the vibration differential equation of the system can be obtained as

$$\hat{\mathbf{M}}\ddot{\mathbf{u}} + \hat{\mathbf{K}}\mathbf{u} = \mathbf{f} \tag{25}$$

where  $\hat{\mathbf{M}}$  and  $\hat{\mathbf{K}}$  are the equivalent mass and stiffness matrices of the improved dynamic model, respectively. When the generalized force vector  $\mathbf{f} = 0$ , the mechanism vibrates freely. According to the improved dynamic model of Equation (25), the improved natural frequency can also be obtained by using Equations (12) and (13).

#### 4. Case Studies and Verification

Two case studies were conducted to verify the matrix displacement model and the improved dynamic model for the distributed-compliance bridge-type amplification mechanism. The first example is a compound distributed-compliance bridge-type amplifier, and the second example is a parallel-guided bridge-type amplifier. The presented modeling methods were also validated by FEA via ANSYS and experimental tests.

##### 4.1. Compound Distributed-Compliance Bridge-Type Amplification Mechanism

The compound distributed-compliance bridge-type displacement amplification mechanism, as shown in Figure 5, was taken as the first case to verify the accuracy of the proposed analytical model. It can be seen intuitively from Figure 5 that the mass of the beam flexures is similar to that of the rigid bodies, so their vibration kinetic energy cannot be ignored in the process of dynamic modeling. In order to reflect the accuracy of the improved dynamic model, the matrix displacement method is also used to model the amplification mechanism for comparison. As shown in Figure 5, the total number of movable rigid bodies in this compound bridge-type amplification mechanism is  $n = 3$ , and the two input forces generated by the PZT are applied to the first and second rigid bodies. The displacement amplification ratio, the input stiffness, and the natural frequency in the working direction are all calculated by the analytical model obtained by the matrix displacement method.

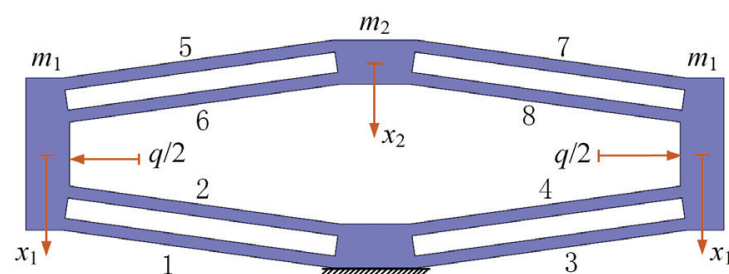


Figure 5. The generalized coordinates of the bridge-type amplifier.

For the improved dynamic modeling, in order to accurately illustrate the motion characteristics of each rigid body in the bridge-type mechanism, the input displacement  $q$  of the bridge-type mechanism and the displacements  $x_1$  and  $x_2$  of rigid bodies 1/2 and 3 in the working direction are taken as the three generalized coordinates of the system, as shown in Figure 5.

According to the selected generalized coordinates, the sum of the kinetic energy of the rigid bodies in the mechanism can be calculated as

$$T_R = \sum_{i=1}^3 T_i = 2 \times \frac{1}{2} m_1 \left[ \left( \frac{\dot{q}}{2} \right)^2 + x_1^2 \right] + \frac{1}{2} m_2 x_2^2 \tag{26}$$

Take Beam 4 as an example: as shown in Figure 6a, the deflections and the angles at both ends are

$$\begin{cases} w_4(0) = 0, \theta_4(0) = w'_4(0) = 0 \\ w_4(l) = x_1 \cos \alpha + (q/2) \cdot \cos \alpha, \theta_4(l) = w'_4(l) = 0 \end{cases} \tag{27}$$

The coefficients of the deflection curve  $w_4(x) = a_{43}x^3 + a_{42}x^2 + a_{41}x + a_{40}$  are

$$\begin{cases} a_{43} = -\frac{2x_1 \cos \theta + q \cos \theta}{l^3} \\ a_{42} = \frac{3}{2} \cdot \frac{2x_1 \cos \theta + q \cos \theta}{l^2} \\ a_{40} = a_{41} = 0 \end{cases} \tag{28}$$

Therefore, the kinetic energy of the four beam flexures 1–4 below can be calculated by Equation (21). Similarly, as shown in Figure 6b, the deflections  $w_6$ , the angles  $\theta_6$ , and the axial displacements  $v_6$  at both ends of Beam Flexure 6 are

$$\begin{cases} w_6(0) = -[x_1 \cos \alpha - (q/2) \cdot \sin \alpha], \theta_6(0) = w'_6(0) = 0 \\ w_6(l) = -x_2 \cos \alpha, \theta_6(l) = w'_6(l) = 0 \\ v_6(0) = -[x_1 \sin \alpha + (q/2) \cdot \cos \alpha], v_6(l) = -x_2 \sin \alpha \end{cases} \tag{29}$$

Therefore, by calculating the coefficients of the deflection equation, the kinetic energy of the upper four beam flexures 5–8 can also be obtained smoothly.

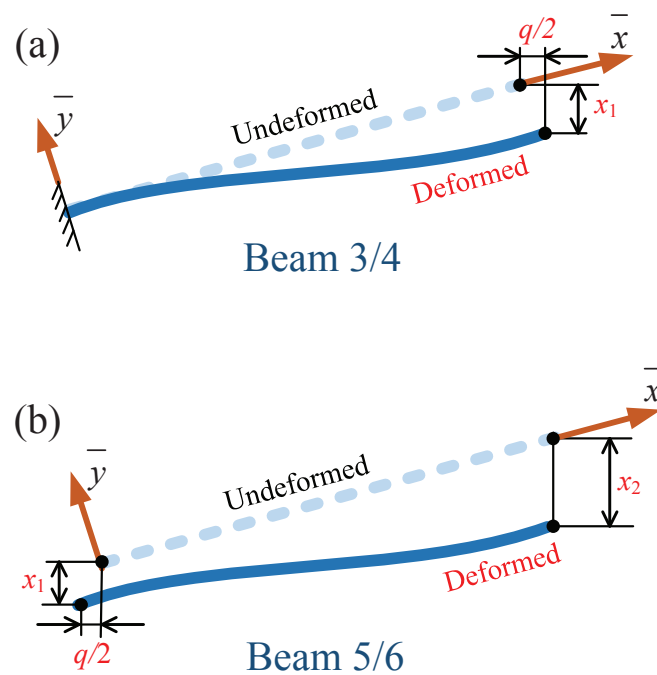


Figure 6. Deformation curves of beam flexures. (a) Beam 3/4. (b) Beam 5/6.

For the potential energy calculation, it can be seen from Figure 6 that the deformation caused by the axial tension or compression of the lower and upper four beams is

$$\begin{aligned}\Delta l_{1-4} &= \frac{q \cos \alpha}{2} - x_1 \sin \alpha \\ \Delta l_{5-8} &= -x_2 \sin \alpha + x_1 \sin \alpha + \frac{q \cos \alpha}{2}\end{aligned}\quad (30)$$

Their section moment is

$$M(x) = EIw'' = EI(6a_3x + 2a_2)\quad (31)$$

Thus, the potential energy of the beam flexures can be calculated by Equation (23). According to the obtained kinetic energy and potential energy of the system, the natural frequency of the mechanism can be obtained by solving the characteristic equation of Equation (25).

For a comprehensive comparison, FEA and an experimental test (Figure 7) were also performed to validate the improved dynamic model. In the experimental setup, a capacitive displacement sensor (NMT.C1) with a resolution of 2.5 nm and a measuring range of 200  $\mu\text{m}$  was used to measure the output displacement of the mechanism. An inductance micrometer (DGG-8Z) with a resolution 0.01  $\mu\text{m}$  was adopted to measure the input displacement of the mechanism. The inductive micrometer and the force sensor (JLBS-MD of Jinnuo company) were combined at the input end of the mechanism for the measurement of the input stiffness of the mechanism. A data acquisition card (PCI-6221) with a 16-bit A/D converter was used to acquire the voltage of the displacement sensor (0–10 V).

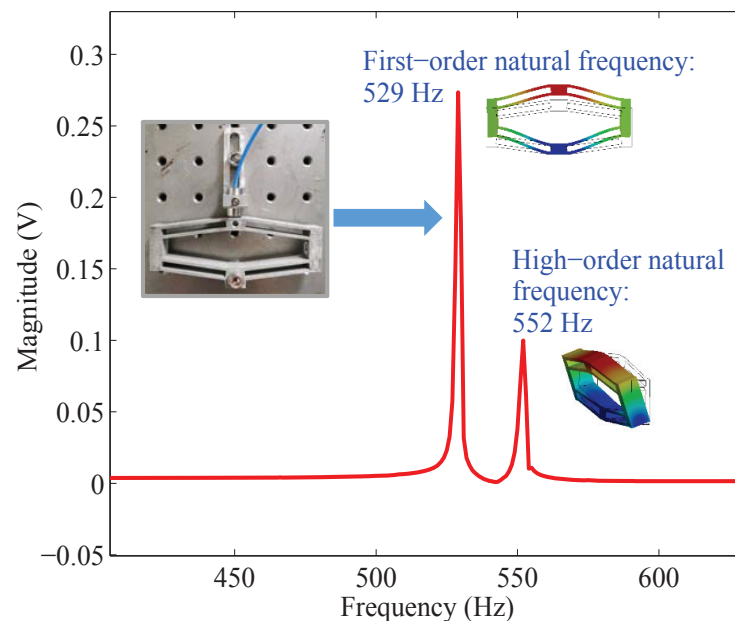


**Figure 7.** Dynamic performance tests of the bridge-type amplifier.

Three samples with different thicknesses  $t$ , widths  $b$ , and lengths  $l$  of the beam flexures, as illustrated in Table 1, were used for the comparisons with the FEA and the experimental results. The material of the mechanism was Aluminum 7075, and its density  $\rho = 2770 \text{ kg/m}^3$ , Young's modulus  $E = 71 \text{ GPa}$ , and Poisson's ratio  $\mu = 0.33$ . The comparison results are listed in Table 1. The comparison results show that, although the static characteristics such as the amplification ratio and input stiffness calculated by the matrix displacement model are relatively accurate, the calculated first-order natural frequency obtained from the matrix displacement method has a large error compared with the FEA and the experimental results, which makes it difficult to be applied to the dynamic performance prediction of distributed-compliance flexure mechanisms. Compared with the

matrix method, the results of the proposed improved dynamic model are much closer to the results of the finite element simulation and experimental test than the matrix displacement model, and its error for Sample 1 is reduced from 50.37% to 2.49% by taking the FEA result as the reference value. Moreover, it can be seen from Table 1 that there are relative large differences between the experimental results and the FEA results, which is mainly attributed to the machining error of the flexure beams.

The error comparisons and variation trends of first-order natural frequencies calculated by matrix displacement model and improved dynamic model for different thicknesses  $t$  of flexure beams are also shown in Figure 8. It can be seen from the figure that with the increase of beam thickness and mass, the error of matrix displacement method becomes much larger, while the error of improved dynamic modeling method is always kept within 8%, which proves the effectiveness of improved dynamic model for distributed-compliance flexure mechanism.

**Table 1.** Comparisons of the static and dynamic performances of the bridge-type amplifier among the analytical, FEA, and testing results.

Sample	Methods	Amplification Ratio	Input Stiffness (N/ $\mu$ m)	1st-Order Nat. Freq. (Hz)	Freq. Error (%)	
1	$l = 40$ mm	Matrix	6.31	19.35	855.13	50.37%
	$b = 12$ mm	FEA	6.24	18.45	568.68	/
	$t = 2$ mm	Test	6.03	16.58	529	/
		Imp. dyn.	/	/	554.51	2.49%
2	$l = 45$ mm	Matrix	6.73	6.14	461.26	37.17%
	$b = 12$ mm	FEA	6.24	5.95	326.27	/
	$t = 1.5$ mm	Test	6.38	4.91	293.54	/
		Imp. dyn.	/	/	301.78	7.5%
3	$l = 45$ mm	Matrix	6.34	18.19	802.31	57.11%
	$b = 12$ mm	FEA	6.28	17.28	510.64	/
	$t = 2.2$ mm	Test	6.07	15.96	484	/
		Imp. dyn.	/	/	488.19	4.39%

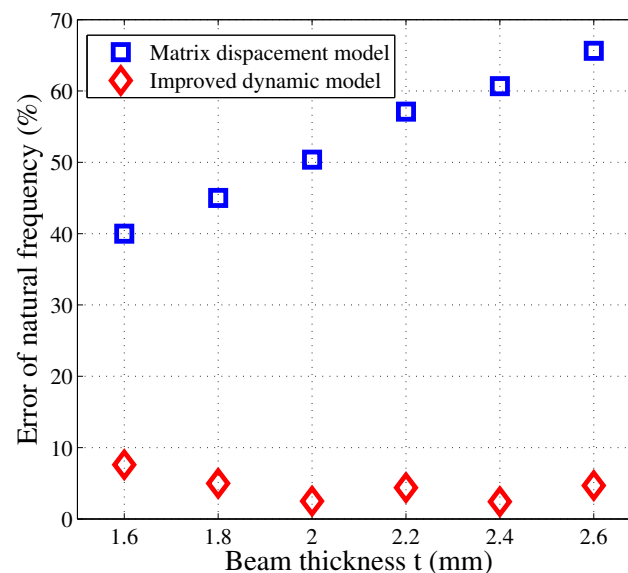


**Figure 8.** Comparison of natural frequency calculation errors.

#### 4.2. Bridge-Type Mechanism Guided by Parallelogram Mechanism

Figure 9 shows a kind of bridge-type displacement amplification mechanism guided by a double-parallelogram mechanism, which was also used to validate the improved dynamic model. The double-parallelogram mechanism was connected with the above compound distributed-compliance bridge-type amplifier above to form the new nanopositioning stage. Both the bridge-type mechanism and the double-parallelogram mechanism use beam

flexures to realize the distributed-compliance. The dimensions of the beam flexures in the bridge-type mechanism were  $t = 2$  mm,  $b = 12$  mm, and  $l = 40$  mm, while those in the parallelogram mechanism were 1.5 mm, 12 mm, and 45 mm, respectively.

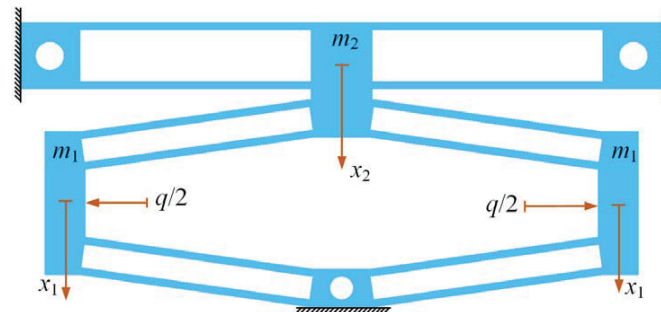


**Figure 9.** Parallel-guided bridge-type amplifier.

As shown in Figure 9, the same generalized coordinates as the analysis of the bridge-type mechanism were selected, and the deflections and rotation angles at both ends of the beam flexures in the parallelogram mechanism are

$$\begin{cases} w(0) = 0, & \theta(0) = w'(0) = 0 \\ w(l) = x_2, & \theta(l) = w'(l) = 0 \end{cases} \quad (32)$$

The calculation results of the natural frequency of the mechanism itself without the PZT are compared in Table 2. The relative errors between the improved dynamic model and FEA results are less than 4%. The accuracy of the natural frequency obtained by the improved dynamic model is greatly increased from 56.8% to 96.4% compared with the matrix model.

**Table 2.** Comparison of the natural frequencies.

Matrix Method (Hz)	Improved Method (Hz)	FEA (Hz)	Test (Hz)
892.36	548.73	569.04	512

## 5. Conclusions

In this paper, the static and dynamic performances of a kind of bridge-type flexure mechanism with distributed-compliance were calculated by using the matrix displacement method and the improved dynamic model. Due to distributed stresses and low mass, this kind of bridge-type distributed-compliance displacement amplification mechanism has much better reliability and dynamic characteristics than the traditional amplification mechanism based on a lumped flexure hinge, especially in high-speed applications. The matrix displacement method was first deduced for the displacement amplification ratio and input stiffness calculations of the bridge-type mechanism. In the modeling method, the stiffness matrix for a free-free flexure beam element was first obtained from its theoretical compliance matrix based on the Timoshenko beam theory. According to the elemental stiffness matrix, the updated stiffness matrix of two rigid bodies connected by the beam flexures can be deduced. The mass centers of two rigid bodies and the forces applied to them are regarded as the node displacement and node forces. By expanding and superimposing each updated elemental stiffness matrix, the global stiffness matrix for the distributed-compliance mechanism can be obtained.

Furthermore, in order to improve the accuracy of the natural frequency calculation by the matrix displacement method, an improved dynamic model was constructed by examining the vibration kinetic energy of beam flexures in the bridge-type distributed-compliance mechanism. Firstly, three generalized coordinates of the distributed-compliance

bridge-type mechanism were selected, and the deflection curve, axial displacement, and rotation angle of the beam flexures were then represented by the generalized coordinates. Then, by deriving the above deformation curves from time, the deflectional, axial, and rotational velocities of each point on the beam flexure can be obtained to calculate the kinetic energy and potential energy in the vibrating beams. Finally, by using the Lagrange method, a three-DOF dynamic equation for the bridge-type mechanism was established to calculate the natural frequency in the working direction.

To verify the accuracy of the analytical model, the FEA and experimental tests for two kinds of distributed-compliance bridge-type mechanism were carried out. The comparisons results showed that the analytical, FEA, and experimental results had high agreement with each other, and the maximum error was less than 8%. It was also shown that, compared with the matrix displacement model, the improved dynamic model can greatly improve the prediction accuracy of the natural frequency, from 56.8% to 96.4%, which has a reference value for the design of the distributed-compliance flexure mechanism and amplified piezoelectric actuator.

**Author Contributions:** P.L. established the analytical model, conceived of and designed the experiments, and wrote the paper; H.Z. constructed the experimental setup; L.L. drew the 3D structure and performed the FEA. All authors have read and agreed to the published version of the manuscript.

**Funding:** This work was supported by the National Natural Science Foundation of China (Grant No. 51605275), Natural Science Foundation of Shanghai (Grant No. 21ZR1426000), and the State Key Laboratory of Mechanical System and Vibration (Grant No. MSV202210).

**Conflicts of Interest:** The authors declare no conflict of interest.

## References

1. Gu, G.Y.; Zhu, L.M.; Su, C.Y.; Ding, H.; Fatikow, S. Modeling and control of piezo-actuated nanopositioning stages: A survey. *IEEE Trans. Autom. Sci. Eng.* **2014**, *13*, 313–332. [[CrossRef](#)]
2. Zhu, W.L.; Zhu, Z.; Shi, Y.; Wang, X.; Guan, K.; Ju, B.F. Design, modeling, analysis and testing of a novel piezo-actuated XY compliant mechanism for large workspace nano-positioning. *Smart Mater. Struct.* **2016**, *25*, 115033. [[CrossRef](#)]
3. Yong, Y.K.; Aphale, S.S.; Moheimani, S.R. Design, identification, and control of a flexure-based XY stage for fast nanoscale positioning. *IEEE Trans. Nanotechnol.* **2008**, *8*, 46–54. [[CrossRef](#)]
4. Choi, K.B.; Lee, J.J.; Hata, S. A piezo-driven compliant stage with double mechanical amplification mechanisms arranged in parallel. *Sens. Actuators Phys.* **2010**, *161*, 173–181. [[CrossRef](#)]
5. Lai, L.J.; Zhu, Z.N. Design, modeling and testing of a novel flexure-based displacement amplification mechanism. *Sens. Actuators Phys.* **2017**, *266*, 122–129. [[CrossRef](#)]
6. Chen, F.; Zhang, Q.; Gao, Y.; Dong, W. A review on the flexure-based displacement amplification mechanisms. *IEEE Access* **2020**, *8*, 205919–205937. [[CrossRef](#)]
7. Chen, G.; Ma, Y.; Li, J. A tensural displacement amplifier employing elliptic-arc flexure hinges. *Sens. Actuators Phys.* **2016**, *247*, 307–315. [[CrossRef](#)]
8. Liu, P.; Yan, P. A new model analysis approach for bridge-type amplifiers supporting nano-stage design. *Mech. Mach. Theory* **2016**, *99*, 176–188. [[CrossRef](#)]
9. Qi, K.Q.; Xiang, Y.; Fang, C.; Zhang, Y.; Yu, C.S. Analysis of the displacement amplification ratio of bridge-type mechanism. *Mech. Mach. Theory* **2015**, *87*, 45–56. [[CrossRef](#)]
10. Ling, M.; Wang, J.; Wu, M.; Cao, L.; Fu, B. Design and modeling of an improved bridge-type compliant mechanism with its application for hydraulic piezo-valves. *Sens. Actuators Phys.* **2021**, *324*, 112687. [[CrossRef](#)]
11. Lobontiu, N.; Garcia, E. Analytical model of displacement amplification and stiffness optimization for a class of flexure-based compliant mechanisms. *Comput. Struct.* **2003**, *81*, 2797–2810. [[CrossRef](#)]
12. Ma, H.W.; Yao, S.M.; Wang, L.Q.; Zhong, Z. Analysis of the displacement amplification ratio of bridge-type flexure hinge. *Sens. Actuators Phys.* **2006**, *132*, 730–736. [[CrossRef](#)]
13. Xu, Q.; Li, Y. Analytical modeling, optimization and testing of a compound bridge-type compliant displacement amplifier. *Mech. Mach. Theory* **2011**, *46*, 183–200. [[CrossRef](#)]
14. Liang, C.; Wang, F.; Huo, Z.; Shi, B.; Tian, Y.; Zhao, X.; Zhang, D. A 2-DOF Monolithic Compliant Rotation Platform Driven by Piezoelectric Actuators. *IEEE Trans. Ind. Electron.* **2020**, *67*, 6963–6974. [[CrossRef](#)]
15. Chen, F.; Du, Z.j.; Yang, M.; Gao, F.; Dong, W.; Zhang, D. Design and analysis of a three-dimensional bridge-type mechanism based on the stiffness distribution. *Precis. Eng.* **2018**, *51*, 48–58. [[CrossRef](#)]
16. Wu, H.; Lai, L.; Zhu, L. Analytical model and experimental verification of an elliptical bridge-type compliant displacement amplification mechanism. *Rev. Sci. Instrum.* **2021**, *92*, 055109. [[CrossRef](#)]

17. Pan, B.; Zhao, H.; Zhao, C.; Zhang, P.; Hu, H. Nonlinear characteristics of compliant bridge-type displacement amplification mechanisms. *Precis. Eng.* **2019**, *60*, 246–256. [[CrossRef](#)]
18. Choi, K.B.; Lee, J.J.; Kim, G.H.; Lim, H.J.; Kwon, S.G. Amplification ratio analysis of a bridge-type mechanical amplification mechanism based on a fully compliant model. *Mech. Mach. Theory* **2018**, *121*, 355–372. [[CrossRef](#)]
19. Chen, J.; Zhang, C.; Xu, M.; Zi, Y.; Zhang, X. Rhombic micro-displacement amplifier for piezoelectric actuator and its linear and hybrid model. *Mech. Syst. Signal Process.* **2015**, *50*, 580–593. [[CrossRef](#)]
20. Letty, R.L.; Claeysen, F.; Lhermet, N.; Bouchilloux, P. New amplified piezoelectric actuator for precision positioning and active damping. In Proceedings of the SPIE 3041, Smart Structures and Materials 1997: Smart Structures and Integrated Systems, San Diego, CA, USA, 6 June 1997; pp. 496–504.
21. Yin, L.; Ananthasuresh, G. Design of distributed compliant mechanisms. *Mech. Based Des. Struct. Mach.* **2003**, *31*, 151–179. [[CrossRef](#)]
22. Sun, Y.; Liu, Y.; Pancheri, F.; Lueth, T.C. LARG: A Lightweight Robotic Gripper With 3-D Topology Optimized Adaptive Fingers. *IEEE/ASME Trans. Mechatron.* **2022**, *27*, 2026–2034. [[CrossRef](#)]
23. Ling, M.; Zhang, X.; Cao, J. Extended dynamic stiffness model for analyzing flexure-hinge mechanisms with lumped compliance. *J. Mech. Des.* **2022**, *144*, 013304. [[CrossRef](#)]
24. Wu, J.; Cai, S.; Cui, J.; Tan, J. A generalized analytical compliance model for cartwheel flexure hinges. *Rev. Sci. Instrum.* **2015**, *86*, 105003. [[CrossRef](#)] [[PubMed](#)]
25. Liu, P.; Yan, P. Kinetostatic modeling of bridge-type amplifiers based on timoshenko beam constraint model. *Int. J. Precis. Eng. Manuf.* **2018**, *19*, 1339–1345. [[CrossRef](#)]
26. Ding, Y.; Lai, L.J. Design and analysis of a displacement amplifier with high load capacity by combining bridge-type and Scott-Russell mechanisms. *Rev. Sci. Instrum.* **2019**, *90*, 065102. [[CrossRef](#)]